UNSYS digital

The Journal of Instrumentation, Automation and Systems

Robust Control of an Unmanned Underwater Vehicle with Parametric Uncertainty

Ismaila Tijani[†], and Agus Budiyono[‡]

[†]Electronics Engineering, ADMC, HCT, United Arab Emirates

[‡]School of Aerospace, Mech. and Manufacturing Eng. Aerospace & Aviation Program, RMIT University, Melbourne, Australia

Abstract—The complex dynamics coupled with operational condition have made an unmanned underwater vehicle susceptible to perturbation due to parametric uncertainty. This has necessitated the need for a robust control technique capable of not only guarantee robustness to unstructured uncertainty, but also account for inherent parametric uncertainty in the system dynamics. This paper presents an optimized based extended H-infinity loop-shaping design procedure for the synthesis of a control system capable of addressing the problem of parametric perturbations in the unmanned underwater vehicle dynamics. The design problem formulation and procedure, together with performance evaluation are highlighted in the paper. Validation of the robustness is examined explicitly using structured singular value analysis.

Keywords—Unmanned underwater vehicle, robust control, extended H-infinity, parametric uncertainty, Multiobjectives Differential Evolution.

I. Introduction

The need for effective guidance and control system (GCS) in the deployment of an unmanned underwater vehicle (UUV) in various applications such as underwater installation inspection and repairs work by offshore company, oceanographic data collection, underwater military surveillance and rescue etc., cannot be underestimated [1]. To this end, several control techniques have been reported in the literatures for GCS development [2-4]. By neglecting the coupling among the system states, classical SISO-based approach such as PID and Fuzzy-PID has been applied as reported in [5-7]. Apart from lack of robustness problem, the limitation of these SISO-based approaches lie in their inability to handle effect of coupling among the states, hence limit the operational range of application. To achieve better robustness and handling coupling in the system dynamics, MIMO-based techniques such as LQR/LQG [8-10], H∞ robust control, [11-12] and intelligent control approach using neural network [13-15] have been reported. Generally, irrespective of the approach adopted, the control scheme is expected to provide not only accurate tracking or navigation, but to robustly stabilize the vehicle in the presence of dynamic perturbation (due to uncertainties).

Among the major sources of the perturbation (unmodeled high frequency dynamics, neglected nonlinearities, use of reduced orders models, and parametric variation), parametric uncertainty is most pervasive due to usual numerical imprecision in the values of various parameters of the system mathematical model and the inherent variation of system parameters to operational conditions and factors. Although as earlier stated, robust techniques especially based on H_∞ approach has been proposed in the literature for the vehicle, little attention has been paid to the problem of parametric uncertainty. Apart from the μ-synthesis (mixed-sensitivity) design method, most of the H_∞ control techniques only guarantee robustness to unstructured uncertainty such as unmodeled dynamics by design. An H controller design using LMI with backstepping control is proposed in [16] for an underwater system with uncertainties and disturbances. The authors reported performance evaluation in the presence of 3% variation in two selected system's parameters. On the other hand, the μ-synthesis approach is noted to be high computationally intensive with many design assumption to be specified [17]. In this paper, a novel robust control approach involving hybrid of the conventional H_∞ Loop Shaping Design Procedures (H_∞ LSDP), *ν*-gap metric with the Multiobjectives Differential Evolution (MODE) is proposed. With this proposed design method, the control problem is formulated as a constrained Multiobjectives optimization problem which captured both the time domain performances, and provides robust stability in the presence of parametric uncertainty. The performance of the technique is evaluated on a longitudinal dynamic of a Squid-like UUV with structured singular value analysis (ssv).

The rest of the paper is organized as follows. Next section presents the system description and mathematical modeling. The overview of the robust control technique is given in Section 3, followed by control problem formulation and applications to UUV system in Section 4. Results, discussion and analysis are given in Section 5, while the paper is concluded in Section 6.

II. System Description and Mathematical Modeling

A biological-inspired, Squid-like AUV structure developed at ITB [18] is adopted as test bed in this study. **Figure 1** shows the AUV system with both fixed Earth inertial coordinate

Corresponding author: Agus Budiyono (e-mail: budiyono@alum.mit.edu).
This paper was submitted on December 09, 2015; revised on December 11, 2015; and accepted on December 27, 2015.

frame, {E} and the moving body coordinate frame, {B} describing the system's coordinate of motion. Based on the kinematics of the system motion, the moving frame, {B} located at the center of gravity of the system, is described by six velocity components, while the frame,{E} consists of six position components, . The descriptions of these components of motion in both reference frames are given in **TABLE I**.

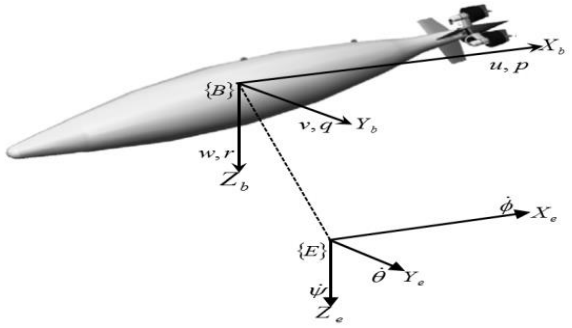

Figure 1 A squid-like Autonomous Underwater (AUV) [18]

TABLE I COMPONENTS OF MOTION IN BOTH BODY AND EARTH REFERENCE FRAMES

Components in Body Frame, {B}	Components in Earth reference frame, {E}
u(t) translational vel. in x-axis	x(t) trans. position in x-axis
v(t) translational vel. in y-axis	y(t) trans. position in y-axis
w(t) trans. (heave) vel. in z-axis	z(t) trans. position in z-axis
p(t) angular velocity in x-axis	ϕ(t) angular rotation in x-axis
q(t) angular velocity in y-axis	θ(t) angular rotation in y-axis
r(t) angular (yaw rate) in z-axis	ψ(t) angular rotation in z-axis

The two frames are related through the following transformation expression:

$$\Gamma = \begin{bmatrix} p \\ q \\ r \end{bmatrix} = \begin{bmatrix} 1 & 0 & -\sin\theta \\ 0 & \cos\phi & \sin\phi\cos\theta \\ 0 & -\sin\phi & \cos\phi\cos\theta \end{bmatrix} \begin{bmatrix} \dot{\phi} \\ \dot{\theta} \\ \dot{\psi} \end{bmatrix} \quad (1)$$

Apart from the kinematic equation in (1), the rigid body equation of motion of the UUV is obtained by contribution of forces and moments due to: (i) inertial, (ii) gravity and Buoyancy, (iii) added mass, (iv) propulsion, (v) steady-states, and (vi) control. The detailed derivation of the system governing equations is reported in [18], while the brief summary is given here for the longitudinal dynamics considered in the control application.

A. Contributing Forces and Moments

In general, the total forces and moments acting on the UUV can be written as:

$$F = F_{G-B} + F_{addedmass} + F_{ss} + F_{prop} + F_{cont}$$

$$M = M_{G-B} + M_{addedmass} + M_{ss} + M_{prop} + M_{cont} \quad (2)$$

The inertial forces and moments: are derived from the Euler-Newton equation:

$$F = \frac{d}{dt}(mU_o) \quad (3)$$

Assuming constant mass, and evaluate the forces with respect to the body frame which moves with respect to the inertial frame, the expression (2) becomes:

$$F = m\left(\left(\frac{dU_o}{dt}\right)_{xyz} + \Gamma + U_o + \frac{d\Gamma}{dt} \times r_G + \Gamma \times (\Gamma \times r_G)\right) \quad (4)$$

where is U_o is the velocity vector, r_G is the position vector of vehicle center of gravity with respect to the body axis. The forces equation in (4) can be decomposed into three scalar components:

$$X = m\left[\dot{u} + wq - vr - x_G\left(q^2 + r^2\right) + y_G(pq - \dot{r}) + z_G(pr + \dot{q})\right]$$

$$Y = m\left[\dot{v} + ur - wp - y_G\left(r^2 + p^2\right) + z_G(qr - \dot{p}) + x_G(qp + \dot{r})\right]$$

$$Z = m\left[\dot{w} + vp - uq - z_G\left(p^2 + q^2\right) + x_G(rp - \dot{q}) + y_G(rp + \dot{p})\right] \quad (5)$$

Similarly, the moment's equations are given as:

$$M_x = p\int_\nabla \left(y^2 + z^2\right)dm - q\int_\nabla xy\, dm - z\int_\nabla xz\, dm$$

$$M_y = -p\int_\nabla xy\, dm + q\int_\nabla \left(z^2 + x^2\right)dm - r\int_\nabla yz\, dm$$

$$M_z = -p\int_\nabla xz\, dm - q\int_\nabla yz\, dm + r\int_\nabla \left(x^2 + y^2\right)dm \quad (6)$$

The forces and moments due to gravity and buoyancy: represents hydrostatic forces and moments acting on the vehicle. Expressed in the body frame, they are given as:

$$F_{G-B} = g(m - \rho\nabla)(-\sin\theta i + \sin\phi\cos\theta j + \cos\phi\cos\theta k) \quad (7)$$

$$\begin{aligned} M_{G-B} = g\{&((my_G - \rho\nabla y_B)\cos\phi\cos\theta - (mz_G - \rho\nabla z_B)\sin\phi\cos\theta)i \\ &-((mz_G - \rho\nabla z_B)\sin\theta + (mx_G - \rho\nabla x_B)\cos\phi\cos\theta)j \\ &-((mx_G - \rho\nabla x_B)\sin\phi\cos\theta + (my_G - \rho\nabla y_B)\sin\theta)k\} \end{aligned} \quad (8)$$

The added mass forces and moments: are due to hydrodynamic force due to acceleration of the vehicle. Generally the added mass is given in terms of tensor with elements A_{ij}, representing the magnitude of the added mass in the *i*-direction due the acceleration in the *j*-direction. The value of *i,j* from 1 to 3 represents the masses associated with surge, sway and heave motion, while those from 4 to 6 represents the moment of inertias associated with roll, pitch and yaw motion. In terms of the equivalent derivative coefficients, the forces and moments are given as:

$$Added\ mass = -\begin{bmatrix} X_{\dot{u}} & 0 & 0 & 0 & 0 & 0 \\ 0 & Y_{\dot{v}} & 0 & 0 & 0 & N_{\dot{v}} \\ 0 & 0 & Z_{\dot{w}} & 0 & M_{\dot{w}} & 0 \\ 0 & 0 & 0 & K_{\dot{p}} & 0 & 0 \\ 0 & 0 & Z_{\dot{q}} & 0 & M_{\dot{q}} & 0 \\ 0 & Y_{\dot{r}} & 0 & 0 & 0 & N_{\dot{r}} \end{bmatrix} \quad (9)$$

The steady state forces and moments: are the result of the viscous fluid effect and are usually calculated based on semi-empirical (empirical) formula or model testing. Using multivariate Taylor series expansion around the equilibrium point, the forces and moments are assumed to be function of velocity as follows:

$$X_s(U_o + u^*, v, w, p, q, r) = X_o + \left(u\frac{\partial}{\partial u} + v\frac{\partial}{\partial v} + w\frac{\partial}{\partial w} + p\frac{\partial}{\partial p} + q\frac{\partial}{\partial q} + r\frac{\partial}{\partial r} \right) X_o + \frac{1}{2!}\left(u\frac{\partial}{\partial u} + v\frac{\partial}{\partial v} + w\frac{\partial}{\partial w} + p\frac{\partial}{\partial p} + q\frac{\partial}{\partial q} + r\frac{\partial}{\partial r} \right)^2 X_o + \ldots \quad (10)$$

where $X_o = X_s(U_o, 0,0,0,0,0)$, and

$$\left(u\frac{\partial}{\partial u} + v\frac{\partial}{\partial v} + w\frac{\partial}{\partial w} + \ldots \right)^2 = u^2\frac{\partial^2}{\partial u^2} + v^2\frac{\partial^2}{\partial v^2} + w^2\frac{\partial^2}{\partial w^2} + \ldots \quad (11)$$

The propulsion forces and moments: are due to the UUV propeller-based thrusters. In the Squid-like vehicle, the thrust, T, is function of velocity U_A, the number of blade, n, fluid density, ρ, and propeller diameter, D:

$$T = \rho\left(n^2 D^4 \tau_o + nD^3 \tau_1 U_A + D^2 \tau_2 U_A^2 + \frac{D\tau_3}{n} U_A^3 \right) \quad (12)$$

and the propulsion forces and moments can be calculated as:

$$X_p = \sum (1 - t_i) T_i \cos(\varepsilon_i)$$

$$X_z = \sum (1 - t_i) T_i \sin(\varepsilon_i)$$

$$M_p = X_p z_p \quad (13)$$

where $U_A = u - uw$.

The control forces and moments: the UUV Squid is control by three differential thrust, $[T_1, T_2, T_3]$, from three different thrusters. Table 2 gives the description of the thruster control for the longitudinal mode. Thruster 2 and 3 can be used simultaneously for the longitudinal mode maneuver, while for the pitch-up or pitch-down maneuver, all three thrusters can also be used simultaneously.

Each thrust can be expressed as:

$$T_i = T_{oi} + \delta T_i \quad (14)$$

In this case, the propulsion force can be expressed as:

$$X_p = \sum X_{p_i} = \sum (1 - t_i)(T_{oi} + \delta T_i) = \sum (1 - t_i) T_{oi} + \sum (1 - t_i) \delta T_i \quad (15)$$

Therefore, the control force and moment are written as:

$$X_c = \sum (1 - t_i) \delta T_i = (1 - t)\delta T_1 + (1 - t)\delta T_2 + (1 - t)\delta T_3 \quad (16)$$

$$M_c = \sum (1 - t_i) \delta T_i \, z_{p_i} \quad i = 1,2,3 = (1 - t)\delta T_1 \, z_{p_1} + (1 - t)\delta T_2 \, z_{p_2} + (1 - t)\delta T_3 \, z_{p_3} \quad (17)$$

TABLE II THRUSTER CONTROL FOR THE LONGITUDINAL MODE

Thruster	Maneuver	Control Input
T_1	Pitch up	reduction of thrust, $-\delta T_1$
	Pitch down	Increase of thrust, $+\delta T_1$
T_2, T_3	Pitch up	Increase of thrust, $+\delta T_{2,3}$
	Pitch down	Reduction of thrust, $-\delta T_{2,3}$

B. Linearized Model for the Longitudinal Dynamics

Combining the above expression for forces and moments, the linearized model of the longitudinal dynamics of the system around operating point of speed, $U_o = 1.5 m/s$ and depth variation, $D = 50m$ is given as:

$$\dot{\bar{x}} = A\bar{x} + B\bar{\delta} \quad (18)$$

where the state vector, $\bar{x} = \{u, v, w, \theta\}$, and the control vector, $\bar{\delta} = \{\delta T_1, \delta T_2, \delta T_3\}$. For the above operating points, the system dynamic matrices A and B are given as []:

$$A = \begin{bmatrix} -0.6122 & 0 & 0 & 0.2935 \\ -0.0019 & -0.5633 & 0.1113 & 0.0066 \\ 0.0570 & 2.4393 & -0.4531 & -0.2014 \\ 0 & 0 & 1 & 0 \end{bmatrix} \quad (19)$$

$$B = \begin{bmatrix} 1.669225E-03 & 1.669225E-03 & 1.669225E-03 \\ 8.90925E-06 & -1.92728E-06 & -1.92728E-06 \\ -2.73863E-04 & 5.9243E-05 & 5.9243E-05 \\ 0 & 0 & 0 \end{bmatrix} \quad (20)$$

This dynamic model is used in the next section for the synthesis of the optimal control proposed in this study, which invariably can be extended to the full system model.

III. OVERVIEW OF THE OPTIMIZED EXTENDED H∞ LSDP

The Extended H_∞ design (E-H_∞LSDP) is a product of integration of the *v*-gap metric with H_∞LSDP design approach [19]. Conventionally, the loop shaping design procedure by McFarlane and Glover [20] accounted for the unstructured

uncertainty on the co-prime factor of the nominal system as shown in **Figure 2**.

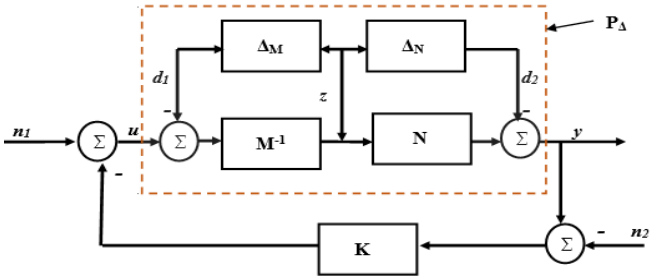

Figure 2 Standard feedback configuration

Expressing the normalized co-prime factor of the nominal plant, P, as $P = NM^{-1}$ where $M^*M + N^*N = I$, the uncertainty plant is given as :

$$P_\Delta = (N + \Delta_N)(M + \Delta_M)^{-1} : \left\| \begin{bmatrix} \Delta_N \\ \Delta_M \end{bmatrix} \right\|_\infty < \frac{1}{\gamma} \ : \ \gamma > 1 \qquad (21)$$

The transfer function of lower system, from d_1, d_2 to z is given by:

$$z = M^{-1}(Ky - d_1) = M^{-1}(K(d_2 - Nz) - d_1)$$

$$\Rightarrow z = (I - M^{-1}KN)^{-1} M^{-1}(Kd_2 - d_1)$$

$$= M^{-1}(I - KP)^{-1}\begin{bmatrix} K & -I \end{bmatrix}\begin{bmatrix} d_2 \\ d_1 \end{bmatrix} \qquad (22)$$

The objective of the H∞LSDP design is to find a stabilizing controller, which maximized the stability margin, $\Psi_{P,K}$ in the face of perturbation to the normalized coprime factor of the plant. Where $\Psi_{P,K}$ is expressed as:

$$\Psi_{P,K} := \begin{cases} \left\| M^{-1}(I - KP)^{-1}\begin{bmatrix} K & -I \end{bmatrix} \right\|_\infty & if\ [P,K]\ is\ stable \\ 0 & otherwise \end{cases} \qquad (23)$$

The above stability criteria is extended to capture robustness to parametric uncertainty measurable by the introduction of the *v*-gap metric into the design procedure. For a nominal plant P_o with parametric variation, δ , and the perturbed plant $P_{\delta_i} : \delta_i \in \delta$. The *v*-gap, $\partial_v(P_o, P_{\delta_i})$, is defined as the maximum possible difference between the closed-loop performance of P_o and P_{δ_i} over a given frequency range and is expressed as:

$$\partial_v(P_o, P_{\delta_i}) = \sup_\omega \frac{|P_o(j\omega) - P_{\delta_i}(j\omega)|}{\sqrt{(1 + |P_o(j\omega)|^2)(1 + |P_{\delta_i}(j\omega)|^2)}} \qquad (24)$$

such that: $0 \le \partial_v(P_o, P_{\delta_i}) < 1$.

The following definition and theorem explain the relationship between the stability margin, $\Psi_{P,K}$ and the v-gap uncertainty measure.

Definition: Given a stabilizing feedback controller K designed for a nominal plant P_o , the achievable optimal stability margin $\Psi_{P_o,K}$ is expressed as:

$$\Psi_{P_o,K} = \frac{|P_o(j\omega) - K(j\omega)|}{\sqrt{(1 + |P_o(j\omega)|^2)(1 + |K(j\omega)|^2)}} \qquad (25)$$

Theorem: For any P_o , and set of perturbed plants P_δ and feedback controller K, let $\sigma = \Psi_{P_o,K}$ and $\alpha = \max_{P_{\delta_i} \in P_\delta} \partial_v(P_o, P_{\delta_i})$, we have

$$\arcsin \Psi_{P_{\delta_i},K} \ge \arcsin \sigma - \arcsin \alpha , \qquad (26)$$

if and only if $P_{\delta_i} \subset P_\delta$

Corollary: If $\Psi_{P_o,K} > \alpha$, then $[P_\delta, K]$ is stable

The implication of theorem 1 in robust controller synthesis is summarized in Lemma 3.1 as follows:

Lemma: Let the nominal shaped plant, $P_{os} = W_2 P_o W_1$ and perturbed shaped plant $P_{\delta s} = W_2 P_\delta W_1$ with input and output weighting functions W_1 and W_2 , respectively:

If $\partial_v(P_{os}, P_{\delta s})$ is small such that $\partial_v(P_{os}, P_{\delta s}) < \varepsilon_{\max}$, for any $\varepsilon > 0$, then any satisfying controller for P_o will also be satisfactory for P_δ and vice-versa, also, if $\partial_v(P_{os}, P_{\delta s})$ is large such that $\partial_v(P_{os}, P_{\delta s}) > \varepsilon_{\max}$ then, there is a satisfactory controller for P_o which perform badly with P_δ and vice-versa.

This extends the performance of a typical H_∞ LSDP in dealing with parametric variation in the system nominal model. The control design problem of an E-H∞LSDP can be stated as follows:

Given a nominal plant P_o , an uncertain set of plants, P_δ , such that, $P_o \in P_\delta$, and all that is known about the "real plant, P " is that, $P \in P_\delta$: the design objective is to find a stabilizing controller K, such that:

$$\sup_K \inf_{P \in P_\delta} \Psi_{P,K} \qquad (27)$$

The first requirement in the design procedure is to compute the chordal radius, r_{P_δ} , which is the maximum distance from the nominal plant, P_o to the boundary of the set, frequency by frequency as follows::

$$r_{P_\delta}(\omega) := \sup_{P \in P_\delta} \aleph(P_o(j\omega), P(j\omega)) \qquad (28)$$

One way is to measure this from frequency response of a finite number of perturbed plants depending on the nature of the set, P_δ. Defining a set of plants:

$$\Gamma(P_o; r_{P_\delta}) := \{P : \partial_\nu(P_o, P) < 1, \aleph(P_o(j\omega), P(j\omega)) \le r_{P_\delta}(\omega) \forall \omega\} \quad (29)$$

And provided, $[P_o, P_\delta]$ is pathwise connected in the graph topology, we have $P \in \Gamma(P_o; r_{P_\delta})$, then $\sup_K \inf_{P \in \Gamma(P_o; r_{P_\delta})} \Psi_{P,K}$ can be easily determined. This is achieved by the controller that uniformly maximizes the stability margin over the enclosed set.

The second design requirement is to determine the appropriate pre- and post- weighting functions, W_1 and W_2 structure and parameters to satisfy the criteria stated in the Lemma above. Based on the above design formulation, W_1 and W_2, should be chosen such that, the $\Psi_{W_1 P W_2, W_2^{-1} K W_1^{-1}}$ achieve the following two design objectives: (i) capture the performance objectives according to conventional loop-shaping technique as reported in [17], and (ii) to make $\partial_\nu(W_1 P_o W_2, W_1 P_{\delta_i} W_2)$ small, for all expected perturbations, $P_{\delta_i} \in P_\delta$. Approaching this using conventional trial and error or technical estimation listed in literature on H_∞-LSDP [17, 21] is noted to be quite difficult for this hybrid robust control technique. Hence, the design procedure is formulated as a constraint Multiobjectives optimization process with the goal of determining optimal weighting functions' parameters that provides sub-optimal compromise between those conflicting design requirements. The detail information on the proposed optimized E-H∞LSDP is given in [19,22].

IV. Controller Design Problem Formulation and Application

This section presents control problem formulation based on the E-H_∞ LSDP given in Section 3, and application to the longitudinal dynamics of the Squid-like UUV presented in Section 2. Given appropriate pre- and post- weighting functions, W_1 and W_2 structure selected prior, the goal of the controller design is to find the set of decision variables in terms of the parameters set, Θ, of the weighting functions W_1 and W_2:

$$\Theta = [w_1, w_2, w_2, ..w_d],\ d = 1..\lambda \quad (30)$$

That yield a stabilizing controller K which satisfies:

$$\sup_K \inf_{P \in P_\delta} \Psi_{P,K}$$

$$\min f_j(\Theta),\ \ j = 1,2,3..\Omega \quad (31)$$

$$L_i \le x_i \le U_i \quad i = 1..\Theta$$

subject to: $g_c(\Theta) \le \beta_c,\ c = 1,2,..N_c$

where $f_k(\Theta)$ is set of objective functions of size Ω, and represents the performance specifications (time domain), $g_c(\Theta)$ is the set of constraints of size N_c with bound specified by the values β_c to be met simultaneously by the parameters, while L and U are the lower and upper bounds on the parameters set, respectively. This constraint Multiobjectives optimization problem is solved using the Multiobjectives Differential Evolution (MODE) algorithm proposed in [22], to yield what is referred to in this study as MODE-based E-H_∞ LSDP. **Figure 3** shows the block diagram of the control synthesis approach conceptually.

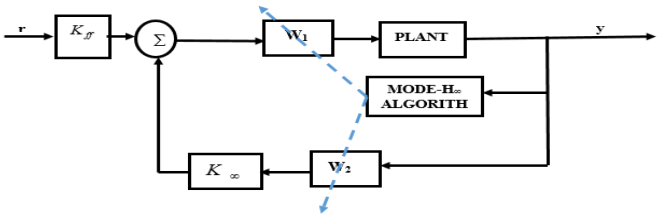

Figure 3 Block diagram of the proposed MODE-based LQR control synthesis

The K_∞ is feedback H_∞ stabilizing controller, while the final controller (shaped controller) is given as:

$$K_s = W_2 K_\infty W_1 \quad (32)$$

The feed forward constant gain, K_{ff} is added to improve the tracking performance [19], and is computed as:

$$K_{ff} = \lim_{s \to 0} K_s W_2 \quad (33)$$

As shown in the **Figure 3**, the performance objective function is given by the response of the full-state feedback system formed for a given decision parameter set. In this study, five control objectives are defined for the pitch angle tracking control as follows:

$$f_j(\Phi) := [t_s^{(\theta)}, OS^{(\theta)}, e_{ss}^{(\theta)}\ {}_{\max} t_s^{(u,w,q)},{}_{,\max} \delta] \quad (34)$$

where $t_s^{(\theta)}$, $OS^{(\theta)}$ and $e_{ss}^{(\theta)}$ are the settling time, percentage overshoot and the steady-state error of the pitch angle, θ, respectively. ${}_{\max} t_s^{(u,w,q)}$ is the maximum off-axis (other states, $\{u, v, w\}$) settling time, and ${}_{\max}\delta$ is the maximum control signal expended. The constraint value is set to account for the ν-gap metric for extended H_∞-LSDP such that $g_c(\Theta) \le \beta_c := \partial_\nu(P_{os}, P_{\delta s}) \le \varepsilon_{\max}^{-1}$

In this study, $\beta_c = 3.0$ in compliance with the minimum condition ($\varepsilon \ge 0.25$) on loop shaping as proposed by [17].

Application to the Unmanned Underwater Vehicle Control

The above control formulation is applied to the longitudinal dynamic of the UUV described in Section 2 with 30% variation in the nominal parameters (i.e. $\delta = 0.3$). Based on the system state-space dynamics (20), and assuming a lead/lag structure for W_1 with integral action added to pitch angle axis for improved steady state response and a constant gain for W_2, such that:

$$W_1 = diag[w_1(s+w_2)/(s+w_3) \quad w_4(s+w_5)/(s+w_6) \quad w_7(s+w_8)/s(s+w_9)]$$

and $W_2 = diag[w_{10} \quad w_{11} \quad w_{12}]$ (35)

The decision variables, Θ in () becomes:

$$\Theta = [w_1, w_2, w_2, ...w_{12}] \quad (36)$$

Therefore, the optimization process was implemented with the following pre-specified parameters: size of decision variables $d = 12$ for twelve parameters; population size, $N_p = 80$; generation size, $G = 10$; cross-over constant, $CR = 0.5$; $\alpha = 50$; lower bound on the decision variables, $L_{1-12} = 0$ and upper bound on the decision variable initiated as, $H_{1-12} = 1$.

Six different runs were carried out to evaluate the repeatability of the algorithm. The final fifty non-dominated solutions for each run are reduced to five using the neighborhood metric described to remove closer solutions. This reduction is carried out in order to ease the final validation of the resulting non-dominated solutions and selection of a controller candidate. Moreover, closer solutions in the Pareto-front tend to have little performance differences that may not affect the overall decision. The final five non-dominated controller candidates together with their performances are shown in **TABLE III** and **IV**, respectively. The comparative response of the five controllers (K1,K2, K3, K4 and K5) is shown in **Figure 4**.

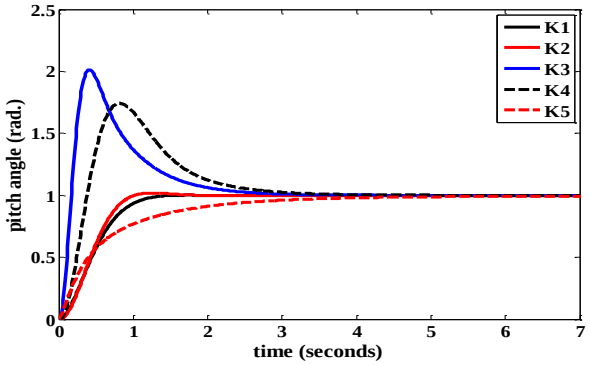

Figure 4 Responses of the five pareto-controllers to 0.2 rad regulator input

All the five non-dominated solutions presented in the **TABLE III** and **IV** and **Figure 4** above are potential robust controller candidates. Selection of the final candidate for implementation is based on the designer priority on the performance objectives as dictated by either experience or additional implementation criteria. A decision matrix is proposed in [22] to guide in the final choice among the Pareto-solutions. In this study, candidate K2 is selected for further analysis and performance validation in the nest section.

V. RESULTS AND DISCUSSION

A MATLAB-Simulink model of the UUV is developed for performance analysis of the selected optimized E- H_∞ LSDP control candidate as shown in **Figure 5**.

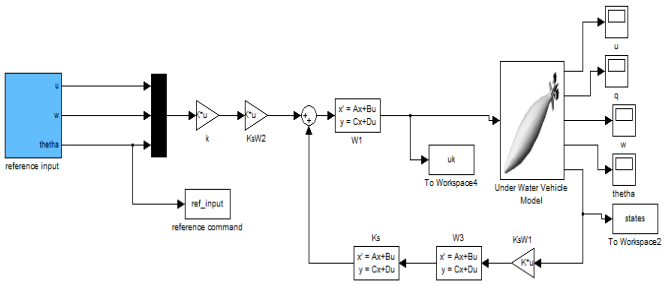

Figure 5 MATLAB-Simulink model for the controller performance evaluation

The tracking performance of the compensator with 10 degree, 0.05Hz square pitch angle command with the nominal plant model is examined. **Figure 6(a-d)** show the response of the pitch angle, forward velocity, pitch rate and vertical velocity, respectively, while the thruster control signal is shown in **Figure 7**. Next, the performance of the compensator in the face of both disturbances (in forward velocity) input (ocean wave) is evaluated. The disturbance V_w is generated based on the following expression, [23]:

$$V_w = \Gamma_{wind}(\mu, \sigma^2) + a\sin(\omega_w t) \quad (37)$$

where $\Gamma_{wind}(\mu, \sigma^2)$ is stochastic process representing the wind turbulence defined by white noise with mean, $\mu = 0$ and variance, σ^2 =0.7. The sinusoidal term represent the wind gust with amplitude, $a = 3.3\,ft/s$ and frequency, $\omega_w = 0.628 rad/s$, **Figure 8** shows the disturbance input generated for the analysis. The comparative responses of the pitch angle, pitch rate, forward velocity and vertical velocity with and without the noise and disturbance input are shown in **Figure 9(a-d).**

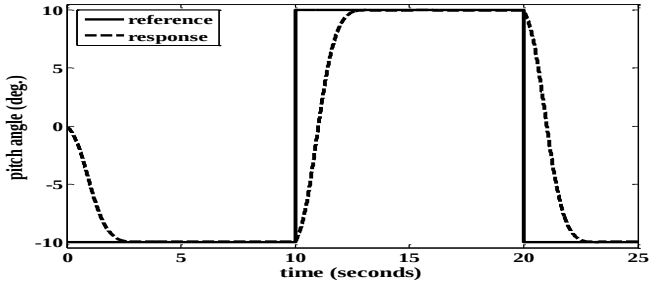

Figure 6a Pitch angle tracking response to 10 deg square input command with nominal plant

TABLE III DECISION PARAMETERS OF FIVE SELECTED CONTROLLER CANDIDATES

	Φ_1	Φ_2	Φ_3	Φ_4	Φ_5	Φ_6	Φ_7	Φ_8	Φ_9	Φ_{10}	Φ_{11}	Φ_{12}
K1	23.62	93.98	99.05	23.84	80.85	94.46	87.90	67.14	48.96	83.96	70.98	66.28
K2	104.47	448.60	54.58	4.18	232.00	194.14	347.38	435.05	108.78	439.40	253.49	323.96
K3	384.55	497.11	10.80	6.77	120.64	339.02	406.99	0.71	478.58	455.33	66.89	350.04
K4	20.87	149.12	473.79	36.44	223.16	263.92	132.99	54.41	41.06	448.15	467.87	476.73
K5	107.90	66.91	477.49	58.94	104.69	468.51	247.93	332.91	472.55	491.60	121.79	431.34

TABLE IV PERFORMANCE OBJECTIVES OF THE FIVE CONTROLLER CANDIDATES

	$t_s^{(\theta)}$	$OS^{(\theta)}$	$\max t_s^{(u,w,q)}$	$\max \beta^{(u,w,q)}$	$\max \delta$	RRNC	RRVG
K1	1.2206	0.1304	0.0001	0.9615	410.3473	2.2674	0.0117
K2	2.6284	101.3464	0.0000	0.1107	24947.7227	2.8948	0.0020
K3	11.7484	0.0000	0.0003	1.0050	886.2954	2.3018	0.0010
K4	0.6472	0.0000	0.0000	1.4067	4093.2812	1.9136	0.0107
K5	0.6005	0.0000	0.0000	1.0730	2681.2168	2.3915	0.0039

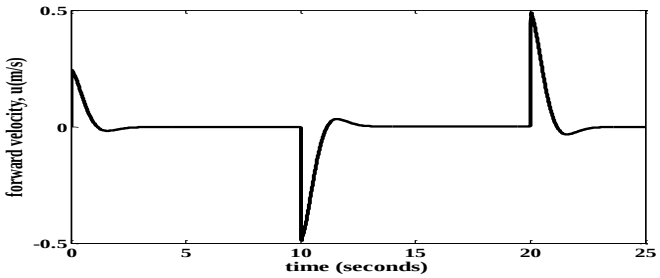

Figure 6b Velocity response to 10 deg square pitch command with nominal plant

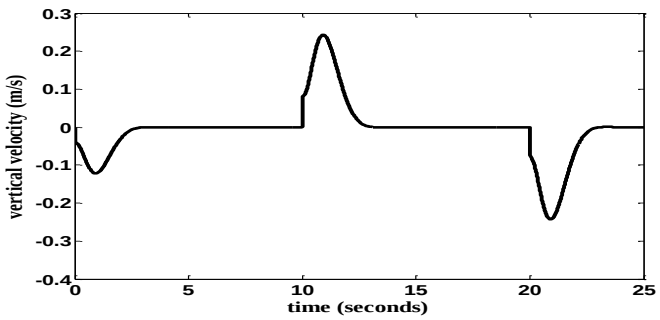

Figure 6d Vertical velocity response to 10 deg square pitch command with nominal plant

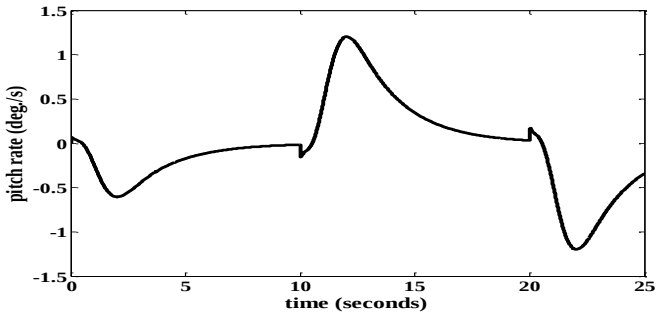

Figure 6c Pitch rate response to 10 deg square pitch command with nominal plant

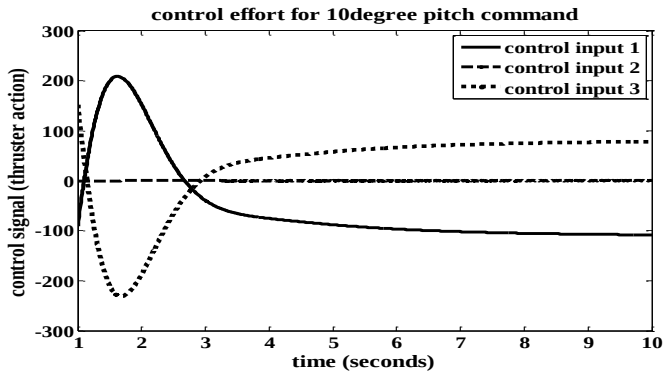

Figure 7 Thruster control for the pitch command with nominal plant

As indicated in **Figure 6a**, the pitch angle command was effectively tracked with system settling time less than 2 seconds, approximately zero tracking error and minimal cross-coupling effect on off-axes responses. The robustness of the compensator to disturbance input is obvious in the **Figure 9** (a-d). Compare to the magnitude of the disturbances as shown in the **Figure 8**, both the transient and steady state responses are not significantly affected. A steady state mean square error of 0.280 in the pitch angle is recorded compare to the response with the nominal system, while the settling remains approximately the same.

The above stability results, $\Psi_{P_{os},K_s} > \partial_v(P_{os}, P_{\delta s})$ sufficiently provides guarantee that the controller is robust to parametric variation according to Lemma stated in the Section 3. However, to validate these results, a structured singular value (*ssv*) analysis is used to examine explicitly the robustness of the close-loop system to uncertainty in the parameter sets.

The *ssv*, $\mu_\Delta(Q)$ is defined as [24]:

$$\mu_\Delta{}^{-1}(Q) := \min_{\Delta\in\prod}\{\bar{\sigma}(\Delta) : \det(I - Q\Delta) = 0\} \qquad (38)$$

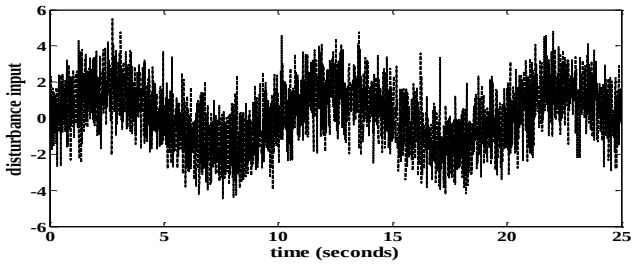

Figure 8 Sample input disturbance

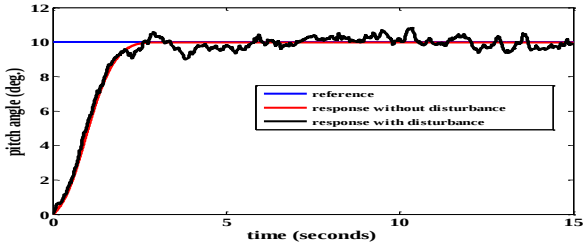

Figure 9a Pitch angle tracking response to 10 deg step input command with and without noise and disturbance input

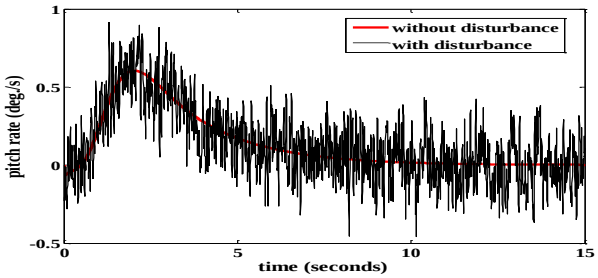

Figure 9b Pitch rates response to 10 deg step input command with and without noise and disturbance input

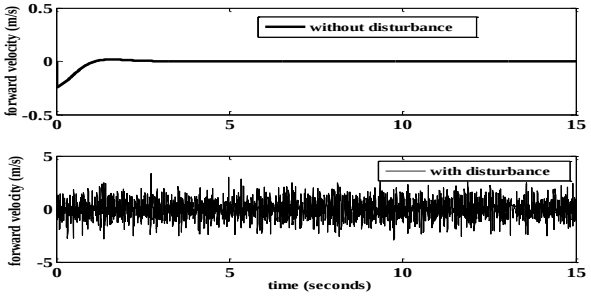

Figure 9c Forward velocity response to 10 deg step input command with and without noise and disturbance input

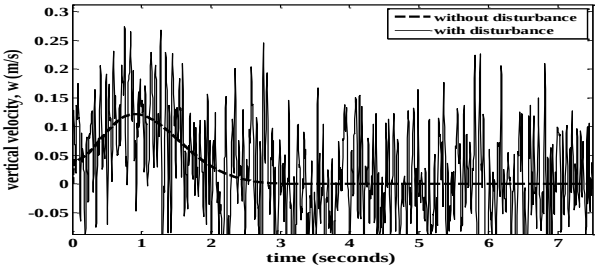

Figure 9d Vertical velocity response to 10 deg step input command with and without noise and disturbance input

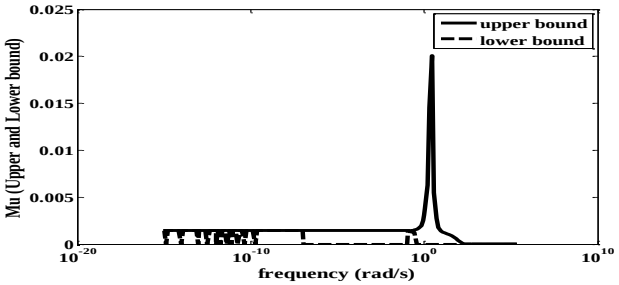

Figure 10 μ plot of robust stability margin

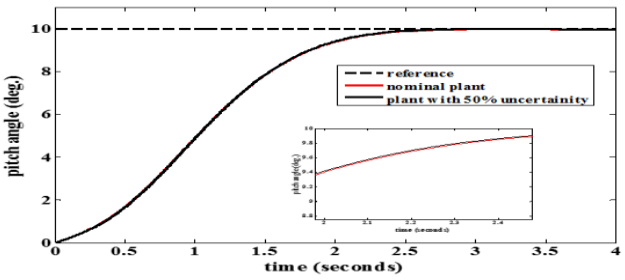

Figure 11a Pitch angle tracking response to 10 deg step input command with and without 30% parametric uncertainty

Figure 10 shows the plot of the robust stability analysis while **TABLE V** presents quantitatively the upper and lower bound on the achieved robustness. As shown in the **Figure 10**, the $\mu_\Delta(Q) < 1$: with lower bound of 0.00145 and upper bound of 0.020, this indicates that the close-loop system is robust to uncertainty model set. The results shown in **TABLE V** further provide insight into the achievable stability margin. The lower bound stability margin of 49.754 implies that the uncertain

system remains stable for all values of uncertain elements up to 4987% outside their modeled uncertain ranges. Comparative time domain responses in **Figure 11** confirmed this robustness with insignificant effect of the parametric perturbation on the plant responses.

TABLE V RESULTS OF ROBUST STABILITY ANALYSIS USING STRUCTURED SINGULAR VALUE (μ ANALYSIS)

	Stability margin
Upper bound	689.109
Lower bound	49.754
Report Uncertain System is robustly stable to modeled uncertainty. -- It can tolerate up to 4975.4% of the modeled uncertainty. -- A destabilizing combination of 68900% of the modeled uncertainty exists, causing an instability at 2.29e-015 rad/s.	

VI. CONCLUSION

The paper has presented the design of a robust controller capable of handling parametric perturbation in an unmanned underwater vehicle dynamics. The proposed design method utilizing an hybrid control scheme involving the conventional H_∞ loop shaping technique, the *v*-gap metric and Pareto-based Multiobjectives differential evolution provides an automated and time saving design approach for such a complex dynamic system compare to the conventional approach. The design method yields set of sub-optimal controller candidates, thereby provides insight into the performance interaction, and options to choose based on actual design goal. The analysis of the optimized E- H_∞ LSDP shows its effectiveness in both tracking and robust performances in the present of both disturbance input and 30% variation in its model parameters. The validation of the robustness with the well-known singular value analysis further strengthens the effectiveness of the proposed technique to provide robust stability for higher variation in the model parameters. The optimization approach involved is expected to facilitate the timely design and deployment of guidance and control algorithm for the unmanned underwater vehicle applications.

REFERENCES

[1] Ura T., AUV 'r2D4', Its Operation, and Road Map for AUV Development, in: *Advances in Unmanned Marine Vehicles*,edited by G.N. Roberts & R. Sutton, (IEE Control Series 69) 2006.

[2] Budiyono, Muljowidodo and A. Sugama, "Coefficient Diagram Method for the Control of an Unmanned Underwater Vehicle," *Indian J Mar Sci*., **38**(3):316-323, Sept. 2009

[3] R. K. Lea, R. Allen and S. L.Merry, "A comparative study of control techniques for an underwater flight vehicle," *International Journal of Systems Science*, volume 30, number 9, 1999, pp. 947- 964. CrossRef

[4] Agus Budiyono, "Advances in unmanned underwater vehicles technologies: Modeling, control and guidance perspectives', Indian J. of Geo-Marine Sciences, October 2009.

[5] Herman, P., Decoupled PD set-point controller for underwater vehicles. *Ocean Engineering*, 2009, vol. 36, no. 6-7, p. 529 to 534.

[6] Wei YH, Peng FG, Sheng C, et al. Control method of the stability of AUV. J Huazhong Univ Sci Technol Nat Sci Ed 2014; 42: 127–132.

[7] Rodrigues, L., Tavares, P., Prado, M. Sliding mode control of an AUV in the diving and steering planes. In *Proceedings of the MTS/IEEE Oceans'06 Conference*. FortLauderdale (FL, USA), 1996, p. 576 - 583. CrossRef

[8] Sabiha A Wadoo, Sadiksha Sapkota, Keerthish Chagachagere, "Optimal Control of an Autonomous Underwater Vehicle', Systems, applications and technology conference (LISAT), 4 May, 2012, IEEE Long Island.

[9] Field, A. I., Cherches, D., Calisal, S. Optimal control of an autonomous underwater vehicle. In *Proceedings of the World Automatic Congress*. Hawaii (USA), 2000, vol. 1, no. 38.

[10] I.B. Tijani and A. Budiyono, (2016). *"Control of an Unmmaned Underwater Vehicles using an Optimized LQR Method"*, Marine and Underwater Science and Technology**,** ISIUS, vol. 1, no. 1, 2016.

[11] Lin-LinWang,Hong-JianWang, and Li-Xin Pan. 'H∞ control for path tracking of autonomous underwater vehicle motion, Advances in Mechanical Engineering2015, Vol. 7(5) 1–1

[12] Triantafyllou M.S. & Grosenbaugh M.A., Robust Control for Underwater Vehicle Systems with Time Delays, *IEEE Journal of Oceanic Engineering*, 16(1991) 146-151. CrossRef

[13] Yuh J., A Neural Net Controller For Underwater Robotic Vehicles, *IEEE Journal of Oceanic Engineering*, 15 (1990), 161-166. CrossRef

[14] Craven, P. J. (1999). Intelligent control strategies for an autonomous underwater vehicle. *PhD Thesis, University of Plymouth, UK*

[15] Ishii K., Fujii T. & Ura T., *Neural network system for online controller adaptation and its application to underwater robot*, (Proceedings of IEEE Int. Conference on Robotics & Automation) 1998, pp. 756–761. CrossRef

[16] Xiaoyu Z., Yuntao H., Tao B., Yanhui W. and Kemao M. (2015). "H Controller design using LMIs for high-speed underwater vehicles in presence of uncertainties and disturbances". Ocean Engineering, Elsevier.

[17] Gu, D., Petko, H. P. & Mihail, M. K. (2005). Robust control design with MATLAB.Springer-Verlag London Limited.

[18] Muljowidodo, Jenie S.D., Budiyono A. & Adinugroho S., Design, Development and Testing of Underwater Vehicles: ITB Experience, paper presented at *The International Conference on Underwater System Technology: Theory and Application*, Penang, Malaysia, 2006.

[19] I.B. Tijani and A. Budiyono,(2016). "Robust Control using an Extended H-Infinity Approach: Concepts and Application",Journal of Mathematics, Statistics and Applications, ISSN: 2288-7113, vol. 1, 2016.

[20] McFarlane, D. & Glover, K., (1990). Robust controller design using normalized coprime factor plant descriptions. Springer Verlag Lecture notes in control and information science series. CrossRef

[21] Stoorvogel, A. A., (1992). *The H∞ control problem: a state space approach*. Department of Electrical Engineering and Computer Science University of Michigan Ann Arbor U.S.A.

[22] Tijani I.B.. Flight control system with MODE based H-infinity for small scale autonomous helicopter. PhD thesis submitted to Mechatronics engineering department, IIUM,Malaysia, October 2012.

[23] Bourhane Kadmiry, (2002), 'Fuzzy Control for an Unmanned Helicopter', PhD thesis, Linköping Studies in Science and Technology, Department of Computer and Information Science, Linköpings Universitet, SE- 581 83 Linköping, Sweden